

Superfluid density and compressibility at the superfluid-Mott glass transition

Cameron Lerch and Thomas Vojta^a

Department of Physics, Missouri University of Science and Technology, Rolla, Missouri 65409, USA

Abstract. Systems of disordered interacting bosons with particle-hole symmetry can undergo a quantum phase transition between the superfluid phase and the Mott glass phase which is a gapless incompressible insulator. We employ large-scale Monte Carlo simulations of a two-dimensional site-diluted quantum rotor model to investigate the properties of the superfluid density and the compressibility at this transition. We find that both quantities feature power-law critical behavior with exponents governed by generalized Josephson relations.

1 Introduction

The physics of systems as diverse as cold atoms in disordered optical lattices [1, 2, 3], superconducting thin films [4, 5], Josephson junction arrays [6, 7], helium absorbed in vycor [8, 9], and doped quantum magnets in large magnetic fields [10, 11, 12] can be described by models of disordered and interacting bosons. These systems can undergo zero-temperature quantum phase transitions between superfluid and insulating ground states.

Because of the disorder, the conventional bulk phases, viz., superfluid and Mott insulator, are separated by a quantum Griffiths phase [13, 14, 15, 16] in which superfluid “puddles” exist in an insulating matrix. Depending on the symmetries, this Griffiths phase can either be a Bose glass or a Mott glass. The Bose glass phase, a compressible gapless insulator, occurs for generic disorder without particle-hole symmetry [17, 18, 19]. If the disordered Hamiltonian is particle-hole symmetric, the glassy phase between the superfluid and the Mott insulator is the incompressible, gapless, and insulating Mott glass (sometimes also called random-rod glass) [20, 21].

The zero-temperature quantum phase transition between superfluid and Mott glass was recently investigated by large-scale Monte Carlo simulations [22, 23], resolving contradictions between earlier predictions [24, 25, 26]. Employing finite-size scaling of the order parameter as well as the correlation length and time, the critical behavior was found to be of conventional power-law type, with universal critical exponents. This agrees with the general classification of phase transitions in disordered systems based on the effective dimensionality of the defects [15, 16, 27].

In the present paper, we focus on the behavior of two experimentally important quantities, the superfluid density ρ_s and the compressibility κ , at this quantum phase transition. By means of Monte Carlo simulations, we establish that both quantities

^a e-mail: vojta@mst.edu

feature power-law critical behavior. The corresponding critical exponents fulfill generalized Josephson relations [18]. The paper is organized as follows: In Sec. 2, we define the model and the quantities under consideration. The Monte-Carlo simulation results are presented in Sec. 3. We conclude in Sec. 4.

2 Quantum rotor model, superfluid density, and compressibility

We consider a square-lattice site-diluted quantum rotor model defined by the Hamiltonian

$$H = \frac{U}{2} \sum_i \epsilon_i \hat{n}_i^2 - J \sum_{\langle ij \rangle} \epsilon_i \epsilon_j \cos(\hat{\phi}_i - \hat{\phi}_j). \quad (1)$$

Here, \hat{n}_i denotes the number operator of lattice site i and $\hat{\phi}_i$ the canonically conjugate phase operator. U and J are the charging energy and the Josephson coupling, respectively, and $\langle ij \rangle$ denotes pairs of nearest neighbor sites. The site dilution is implemented via the independent quenched random variables ϵ_i that can take the values 0 (vacancy) with probability p and 1 (occupied site) with probability $1 - p$. If the filling, i.e., the average particle number $\langle n \rangle$, is an integer then the Hamiltonian is particle-hole symmetric, which is the case we focus on in the following. The qualitative behavior of the rotor model (1) is easily understood: If the charging energy dominates, $U \gg J$, the ground state is Mott-insulating. For $U \ll J$ and dilutions below the percolation threshold, the ground state is superfluid.

We now map the quantum rotor Hamiltonian (1) onto a classical (2+1)-dimensional XY model [28] with columnar defects,

$$H_{\text{cl}} = -J_s \sum_{\langle i,j \rangle, t} \epsilon_i \epsilon_j \mathbf{S}_{i,t} \cdot \mathbf{S}_{j,t} - J_\tau \sum_{i,t} \epsilon_i \mathbf{S}_{i,t} \cdot \mathbf{S}_{i,t+1}. \quad (2)$$

Here i denotes a position in two-dimensional real space, and t is the ‘‘imaginary time’’ coordinate. $\mathbf{S}_{i,t}$ is an O(2) unit vector. The values of the classical interactions J_s/T and J_τ/T depend on the parameters of the quantum Hamiltonian (1). The classical temperature T differs from the real physical temperature T_Q which is zero at the quantum phase transition. As the critical behavior is expected to be universal, we fix $J_s = J_\tau = 1$ and tune the transitions by varying the classical temperature T .

Under the quantum-to-classical mapping, the compressibility $\kappa = \partial \langle n \rangle / \partial \mu$ of the quantum rotor Hamiltonian (1) maps onto the spinwave stiffness in the imaginary time direction

$$\rho_{\text{cl},\tau} = L_\tau^2 (\partial^2 f / \partial \Theta^2)_{\Theta=0} \quad (3)$$

of the XY model (2) (up to constant factors). Here, L_τ is the system size in imaginary time direction, and f is the free energy density for twisted boundary conditions (the XY spins $\mathbf{S}_{i,t}$ at $t = 0$ make an angle of Θ with those at $t = L_\tau$). Analogously, the superfluid density ρ_s of the quantum rotor model maps onto the spinwave stiffness

$$\rho_{\text{cl},s} = L^2 (\partial^2 f / \partial \Theta^2)_{\Theta=0} \quad (4)$$

in the space direction of the XY model, with L being the spatial linear system size. (The twisted boundary conditions are now applied in x or y direction.)

3 Monte Carlo simulations

We perform Monte Carlo simulations of the classical XY model (2) combining Wolff [29] and Metropolis updates [30]. Wolff cluster updates greatly reduce critical slowing

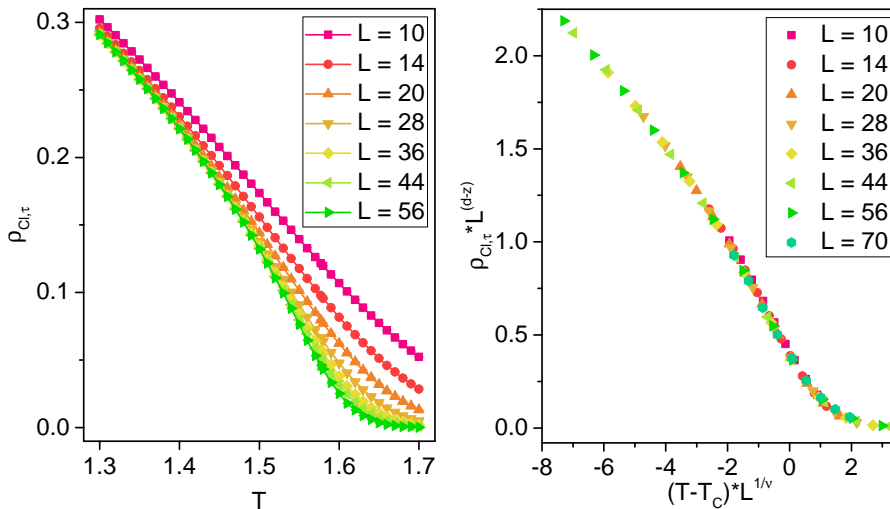


Fig. 1. Left: Stiffness $\rho_{cl,\tau}$ in imaginary time direction vs. classical temperature T for various systems sizes. The dilution is $p = 1/3$. The statistical errors of the data are smaller than the symbol size. Right: Scaling plot of $\rho_{cl,\tau}$ according to eq. (5).

down while Metropolis single-spin updates help equilibrate disconnected clusters that occur in a diluted lattice. We study a dilution of $p = 1/3$ because it was found to lead to small corrections to scaling at the disordered critical point [22]. For comparison, we also analyze the clean case, $p = 0$. System sizes range from $L = 10$ to 84 in the space directions and from $L_\tau = 14$ to 348 in imaginary time direction. All data are averaged over 10,000 disorder configurations. The equilibration period is 200 Monte Carlo sweeps for each sample, and the measurement period is 500 sweeps, with a measurement taken after each sweep. (Performing short Monte Carlo runs for a large number of disorder configurations reduces the overall statistical error [31,32,33,34,35]).

We compute the temporal and spatial stiffnesses $\rho_{cl,\tau}$ and $\rho_{cl,s}$ by employing numerical estimators that can be evaluated in conventional Monte Carlo runs without actually having to apply twisted boundary conditions [36]. To test our algorithms, we first analyze the clean case, $p = 0$, using systems with up to 224^3 sites. As the clean system is isotropic, $\rho_{cl,\tau}$ and $\rho_{cl,s}$ agree with each other. At the critical temperature, $T_c = 2.201844$ [22], they decay as L^{-1} with system size, as predicted by the Josephson scaling relation $\rho_{cl} \sim L^{2-d_{cl}}$ [37]. Here, $d_{cl} = d + 1 = 3$ is the total dimensionality of the classical XY model (2).

We now turn to the main results of this paper, viz., the behavior of $\rho_{cl,\tau}$ and $\rho_{cl,s}$ in the disordered case, $p = 1/3$. As the disorder breaks the symmetry between space and imaginary time, L and L_τ are not equivalent, and we need to perform anisotropic finite-size scaling. The optimal sample shapes for the present simulations as well as the value of the critical temperature, $T_c = 1.577$, are taken from Ref. [22]. The left panel of Fig. 1 presents an overview of the temporal stiffness $\rho_{cl,\tau}$ for several system sizes. As expected, $\rho_{cl,\tau}$ approaches a nonzero value for $T < T_c$ (superfluid phase) while it decays towards zero for $T > T_c$ (Mott glass phase). The spatial stiffness $\rho_{cl,s}$ behaves in a similar fashion.

To determine the critical behavior of the stiffnesses $\rho_{cl,\tau}$ and $\rho_{cl,s}$ quantitatively, we analyze their system-size dependence at the critical temperature $T_c = 1.577$ in Fig. 2. The figure demonstrates that both stiffnesses feature power-law behavior, $\rho_{cl,\tau} \sim L^{-y_\tau}$ and $\rho_{cl,s} \sim L^{-y_s}$ where y_τ and y_s are the scale dimensions of the

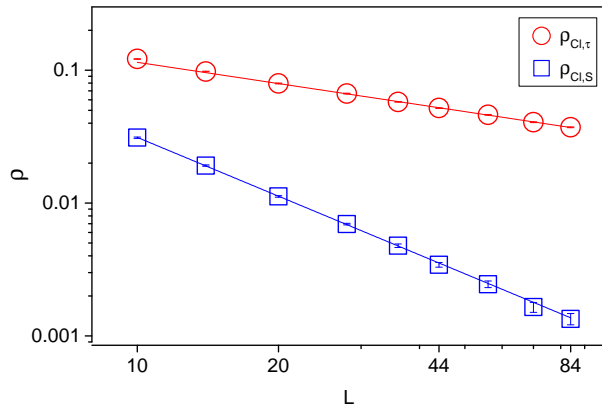


Fig. 2. Double logarithmic plot of the spinwave stiffnesses $\rho_{cl,\tau}$ and $\rho_{cl,s}$ at the critical temperature $T_c = 1.577$ as functions of the spatial linear system size L . The solid lines are power-law fits to $\rho_{cl,\tau} \sim L^{-y_\tau}$ and $\rho_{cl,s} \sim L^{-y_s}$.

stiffnesses. Power-law fits yield the values $y_\tau = 0.53(5)$ and $y_s = 1.47(6)$. The errors (indicated by the numbers in parentheses) mostly stem from the uncertainty of T_c ; the statistical errors are much smaller. According to the generalized Josephson relations [18], y_τ and y_s should fulfill the exponent equalities $y_\tau = d - z$ and $y_s = d + z - 2$. Using $d = 2$ and the estimate $z = 1.52(3)$ from Ref. [22], we see that both relations are fulfilled within their error bars.

A more complete analysis of the critical behavior is provided by testing the scaling behavior of the stiffnesses. The scaling form of the temporal stiffness reads

$$\rho_{cl,\tau}(r, L) = L^{-y_\tau} X_\tau(rL^{1/\nu}) \quad (5)$$

where $\nu = 1.16$ [22] is the correlation length exponent, $r = T - T_c$ denotes the distance from criticality, and X_τ is a universal scaling function. The right panel of Fig. 1 shows that our data fulfill the scaling form with high accuracy. The spatial stiffness can be analyzed in a similar manner.

4 Conclusions

Couched in terms of the original disordered boson problem, i.e., the quantum rotor Hamiltonian (1), our findings can be summarized as follows: Close to the superfluid-Mott glass quantum phase transition, the compressibility and the superfluid density display power-law critical behavior, $\kappa \sim L^{-y_\tau}$ and $\rho_s \sim L^{-y_s}$. The scale dimensions $y_\tau = 0.53(5)$ and $y_s = 1.47(6)$ fulfill the generalized Josephson relations, $y_\tau = d - z$ and $y_s = d + z - 2$, within their error bars.

Combining these results with the critical exponents determined in Ref. [22], we can write down the full scaling forms of κ and ρ_s as functions of the distance r from criticality, temperature T_Q , and system size L ,

$$\kappa(r, T_Q, L) = b^{-y_\tau} \kappa(rb^{1/\nu}, T_Q b^z, Lb^{-1}), \quad (6)$$

$$\rho_s(r, T_Q, L) = b^{-y_s} \rho_s(rb^{1/\nu}, T_Q b^z, Lb^{-1}). \quad (7)$$

Here, b is an arbitrary length scale factor. (Recall that T_Q is the physical temperature of the quantum system, not the classical temperature T appearing in the mapped classical XY model.)

Potential experimental realizations of Mott glass physics can be found, e.g., in granular superconductors, ultracold atoms, and certain magnetic systems [38]. The last example is particularly promising as the necessary particle-hole symmetry arises naturally in the absence of a magnetic field.

This work was supported in part by the NSF under Grant Nos. DMR-1506152 and PHY-1125915. T.V. is grateful for the hospitality of the Kavli Institute for Theoretical Physics, Santa Barbara, where part of the work was performed.

References

1. M. White, M. Pasienski, D. McKay, S.Q. Zhou, D. Ceperley, B. DeMarco, *Phys. Rev. Lett.* **102**, 055301 (2009)
2. S. Krinner, D. Stadler, J. Meineke, J.P. Brantut, T. Esslinger, *Phys. Rev. Lett.* **110**, 100601 (2013)
3. C. D’Errico, E. Lucioni, L. Tanzi, L. Gori, G. Roux, I.P. McCulloch, T. Giamarchi, M. Inguscio, G. Modugno, *Phys. Rev. Lett.* **113**, 095301 (2014)
4. D.B. Haviland, Y. Liu, A.M. Goldman, *Phys. Rev. Lett.* **62**, 2180 (1989)
5. A.F. Hebard, M.A. Paalanen, *Phys. Rev. Lett.* **65**, 927 (1990)
6. H.S.J. van der Zant, F.C. Fritschy, W.J. Elion, L.J. Geerligs, J.E. Mooij, *Phys. Rev. Lett.* **69**, 2971 (1992)
7. H.S.J. van der Zant, W.J. Elion, L.J. Geerligs, J.E. Mooij, *Phys. Rev. B* **54**, 10081 (1996)
8. B.C. Crooker, B. Hebral, E.N. Smith, Y. Takano, J.D. Reppy, *Phys. Rev. Lett.* **51**, 666 (1983)
9. J.D. Reppy, *Physica B+C* **126**, 335 (1984)
10. A. Oosawa, H. Tanaka, *Phys. Rev. B* **65**, 184437 (2002)
11. T. Hong, A. Zheludev, H. Manaka, L.P. Regnault, *Phys. Rev. B* **81**, 060410 (2010)
12. R. Yu, L. Yin, N.S. Sullivan, J.S. Xia, C. Huan, A. Paduan-Filho, N.F. Oliveira Jr, S. Haas, A. Steppke, C.F. Miclea et al., *Nature* **489**, 379 (2012)
13. R.B. Griffiths, *Phys. Rev. Lett.* **23**, 17 (1969)
14. M. Thill, D.A. Huse, *Physica A* **214**, 321 (1995)
15. T. Vojta, *J. Phys. A* **39**, R143 (2006)
16. T. Vojta, *J. Low Temp. Phys.* **161**, 299 (2010)
17. D.S. Fisher, M.P.A. Fisher, *Phys. Rev. Lett.* **61**, 1847 (1988)
18. M.P.A. Fisher, P.B. Weichman, G. Grinstein, D.S. Fisher, *Phys. Rev. B* **40**, 546 (1989)
19. L. Pollet, N.V. Prokof’ev, B.V. Svistunov, M. Troyer, *Phys. Rev. Lett.* **103**, 140402 (2009)
20. T. Giamarchi, P. Le Doussal, E. Orignac, *Phys. Rev. B* **64**, 245119 (2001)
21. P.B. Weichman, R. Mukhopadhyay, *Phys. Rev. B* **77**, 214516 (2008)
22. T. Vojta, J. Crewse, M. Puschmann, D. Arovas, Y. Kiselev, *Phys. Rev. B* **94**, 134501 (2016)
23. M. Puschmann, T. Vojta, *J. Phys. Conf. Series* **905**, 012038 (2017)
24. N. Prokof’ev, B. Svistunov, *Phys. Rev. Lett.* **92**, 015703 (2004)
25. S. Iyer, D. Pekker, G. Refael, *Phys. Rev. B* **85**, 094202 (2012)
26. M. Swanson, Y.L. Loh, M. Randeria, N. Trivedi, *Phys. Rev. X* **4**, 021007 (2014)
27. T. Vojta, J. Schmalian, *Phys. Rev. B* **72**, 045438 (2005)
28. M. Wallin, E.S. Sorensen, S.M. Girvin, A.P. Young, *Phys. Rev. B* **49**, 12115 (1994)
29. U. Wolff, *Phys. Rev. Lett.* **62**, 361 (1989)
30. N. Metropolis, A. Rosenbluth, M. Rosenbluth, A. Teller, *J. Chem. Phys.* **21**, 1087 (1953)
31. H.G. Ballesteros, L.A. Fernández, V. Martín-Mayor, A. Muñoz Sudupe, G. Parisi, J.J. Ruiz-Lorenzo, *Phys. Rev. B* **58**, 2740 (1998)
32. H.G. Ballesteros, L.A. Fernandez, V. Martin-Mayor, A. Munoz Sudupe, G. Parisi, J.J. Ruiz-Lorenzo, *Nucl. Phys. B* **512**, 681 (1998)
33. R. Sknepnek, T. Vojta, M. Vojta, *Phys. Rev. Lett.* **93**, 097201 (2004)
34. T. Vojta, R. Sknepnek, *Phys. Rev. B* **74**, 094415 (2006)
35. Q. Zhu, X. Wan, R. Narayanan, J.A. Hoyos, T. Vojta, *Phys. Rev. B* **91**, 224201 (2015)
36. S. Teitel, C. Jayaprakash, *Phys. Rev. B* **27**, 598 (1983)
37. B.D. Josephson, *Phys. Rev. Lett.* **21**, 608 (1966)
38. T. Roscilde, S. Haas, *Phys. Rev. Lett.* **99**, 047205 (2007)